JOURNAL OF MAGNETIC RESONANCE, Series B 106, 92–96 (1995)

The Impact of Direct Refinement against $^{13}C^{\alpha}$ and $^{13}C^{\beta}$ Chemical Shifts on Protein Structure Determination by NMR

JOHN KUSZEWSKI, JUN QIN, ANGELA M. GRONENBORN,* AND G. MARIUS CLORE*

Laboratory of Chemical Physics, Building 5, National Institute of Diabetes and Digestive and Kidney Diseases, National Institutes of Health, Bethesda, Maryland 20892-0520

Received October 6, 1994

Recent studies have revealed a clear empirical correlation between the protein backbone conformation (defined in terms of the ϕ and ψ torsion angles) and the $^{13}C^{\alpha}$ and $^{13}C^{\beta}$ secondary chemical shifts (that is, the difference between observed shifts and random coil shifts) (*1–3*). In addition, *ab initio* quantum-mechanical calculations have indicated that the ϕ, ψ angles dominate shielding for C^{α} and C^{β} atoms (*4, 5*). With these findings, it seemed worthwhile to incorporate $^{13}C^{\alpha}$ and $^{13}C^{\beta}$ chemical shifts directly into the refinement of protein structures determined by NMR, in a manner analogous to that recently described for $^{3}J_{HN\alpha}$ coupling constants (*6*).

The strategy that we employed makes use of the empirical surface describing the expected C^{α} and C^{β} secondary chemical shifts as a function of the backbone torsion angles ϕ and ψ, published by Spera and Bax (*1*). This surface, which was derived from a set of four proteins whose ^{13}C chemical shifts were known and for which high-resolution crystal structures were available, was generated as follows. The crystallographic dihedral angles and the NMR secondary shifts for nondisordered residues from these proteins were first combined to give a set of data points, each having information on ϕ and ψ, and C^{α} and C^{β} secondary shifts. To facilitate the conversion of these data points into a surface of expectation values, the total space of ϕ and ψ (from $-180°$ to $+180°$ for each angle) was divided into a grid of 32,400 points, with each grid point representing a 2° by 2° square in ϕ, ψ space. This set of data points was then converted into expected C^{α} and C^{β} secondary shifts at each grid point via a procedure in which data points contribute to the expectation value of several grid points nearest any given data point's ϕ and ψ values. Specifically, the weight given to each of the data points in this average drops off as a Gaussian function of the distance from the particular grid point to the data point such that (*1*)

$$C^{\alpha}_{\text{expected}}(\phi, \psi) = \{\sum C^{\alpha}_{k}(\phi_k, \psi_k)\exp[-((\phi - \phi_k)^2 + (\psi - \psi_k)^2)/S]\} / \{\sum \exp[-((\phi - \phi_k)^2 + (\psi - \psi_k)^2)/S]\}, \quad [1]$$

and similarly for $C^{\beta}_{\text{expected}}$. S is the Gaussian scale factor given by $r^2/e^{0.5}$, where r is the radius of the Gaussian (in this case $r = 17.7°$ and $S = 450$). Expectation values were published only for those grid points where the residue density function, $\sum \exp[-((\phi - \phi_k)^2 + (\psi - \psi_k)^2)/S]$, was greater than 3.1. The rms deviation of the starting data points to each expected secondary shift was also calculated at each grid point to provide an estimate of the error in the expected secondary shifts at each grid point.

In order to refine directly against $^{13}C^{\alpha}$ and $^{13}C^{\beta}$ secondary chemical shifts, we incorporated a carbon chemical-shift energy term into the simulated-annealing program XPLOR (*7, 8*) by means of the following approach. Given a set of atomic coordinates, the expected secondary carbon shifts for the C^{α} and C^{β} atoms, $C^{\alpha}_{\text{expected}}$ and $C^{\beta}_{\text{expected}}$, of a given residue were determined by locating the grid point closest to that residue's ϕ and ψ angles and looking up the expected shifts from the Spera and Bax (*1*) empirical surface. A carbon-shift "energy" term, E_{Cshift}, for that residue was then calculated from the expectation values and the observed secondary shifts, $C^{\alpha}_{\text{observed}}$ and $C^{\beta}_{\text{observed}}$, as either a harmonic potential or a square-well potential. The harmonic potential is given by

$$E_{\text{Cshift}}(\phi, \psi) = k_{\text{Cshift}}[(\Delta C^{\alpha}(\phi, \psi))^2 + (\Delta C^{\beta}(\phi, \psi))^2], \quad [2]$$

where

$$\Delta C^{n}(\phi, \psi) = C^{n}_{\text{expected}}(\phi, \psi) - C^{n}_{\text{observed}} \quad (n = \alpha \text{ or } \beta) \quad [3]$$

* Authors to whom correspondence should be addressed.

1064-1866/95 $6.00

and k_{Cshift} is a force constant. The square-well potential is given by

$$E_{Cshift}(\phi, \psi) = k_{Cshift}[(\Delta C^{\alpha}_{e}(\phi, \psi))^2 + (\Delta C^{\beta}_{e}(\phi, \psi))^2], \quad [4]$$

where

$$\Delta C^{\alpha}_{e}(\phi, \psi) = \begin{cases} |\Delta C^{\alpha}(\phi, \psi)| - \text{error}^{\alpha}(\phi, \psi), & \text{if } |\Delta C^{\alpha}(\phi, \psi)| > \text{error}^{\alpha}(\phi, \psi) \\ 0, & \text{if } |\Delta C^{\alpha}(\phi, \psi)| \leq \text{error}^{\alpha}(\phi, \psi) \end{cases} \quad [5]$$

$$\Delta C^{\beta}_{e}(\phi, \psi) = \begin{cases} |\Delta C^{\beta}(\phi, \psi)| - \text{error}^{\alpha}(\phi, \psi), & \text{if } |\Delta C^{\beta}(\phi, \psi)| > \text{error}^{\beta}(\phi, \psi) \\ 0, & \text{if } |\Delta C^{\beta}(\phi, \psi)| \leq \text{error}^{\beta}(\phi, \psi) \end{cases} \quad [6]$$

and $\text{error}^{\alpha}(\phi, \psi)$ and $\text{error}^{\beta}(\phi, \psi)$ are the rms deviations of the experimental database from the expectation values of the C^{α} and C^{β} secondary shifts, respectively, at the grid point (ϕ, ψ), obtained by Spera and Bax (*1*).

In order to use molecular dynamics or conjugate-gradient minimization techniques to improve the agreement of the observed and expected carbon chemical shifts, the partial derivatives of the energy along ϕ and ψ (i.e., the forces along ϕ and ψ) must also be calculated. Differentiating by the chain rule, the harmonic forces are given by

$$\delta E_{Cshift}/\delta\phi(\phi, \psi) = 2k_{Cshift}\{[(\Delta C^{\alpha}(\phi, \psi))\delta C^{\alpha}_{expected}/\delta\phi] + [(\Delta C^{\beta}(\phi, \psi))\delta C^{\beta}_{expected}/\delta\phi]\} \quad [7]$$

and

$$\delta E_{Cshift}/\delta\psi(\phi, \psi) = 2k_{Cshift}\{[(\Delta C^{\alpha}(\phi, \psi))\delta C^{\alpha}_{expected}/\delta\psi] + [(\Delta C^{\beta}(\phi, \psi))\delta C^{\beta}_{expected}/\delta\psi]\}. \quad [8]$$

Similarly, defining

$$\Delta C^{n}_{sign} = \Delta C^{n}(\phi, \psi)/|\Delta C^{n}(\phi, \psi)|, \quad [9]$$

the square-well forces are given by

$$\delta E_{Cshift}/\delta\phi(\phi, \psi) = 2k_{Cshift}\{[(\Delta C^{\alpha}_{sign})(|\Delta C^{\alpha}(\phi, \psi)| - \text{error}^{\alpha}(\phi, \psi))\delta C^{\alpha}_{expected}/\delta\phi] + [(\Delta C^{\beta}_{sign})(|\Delta C^{\beta}(\phi, \psi)| - \text{error}^{\beta}(\phi, \psi))\delta C^{\beta}_{expected}/\delta\phi]\} \quad [10]$$

$$\delta E_{Cshift}/\delta\psi(\phi, \psi) = 2k_{Cshift}\{[(\Delta C^{\alpha}_{sign})(|\Delta C^{\alpha}(\phi, \psi)| - \text{error}^{\alpha}(\phi, \psi))\delta C^{\alpha}_{expected}/\delta\psi] + [(\Delta C^{\beta}_{sign})(|\Delta C^{\beta}(\phi, \psi)| - \text{error}^{\beta}(\phi, \psi))\delta C^{\beta}_{expected}/\delta\psi]\} \quad [11]$$

if $|\Delta C^{\alpha}(\phi, \psi)| > \text{error}^{\alpha}(\phi, \psi)$ and $|\Delta C^{\beta}(\phi, \psi)| > \text{error}^{\beta}(\phi, \psi)$, otherwise $\delta E_{Cshift}/\delta\phi(\phi, \psi) = 0$. Just as in the case of the calculation of the square-well energy term (Eqs. [4]–[6]), if the difference between the observed and the expected chemical-shift values for one of the carbon atoms is within its error, but that for the other carbon is not, the partial

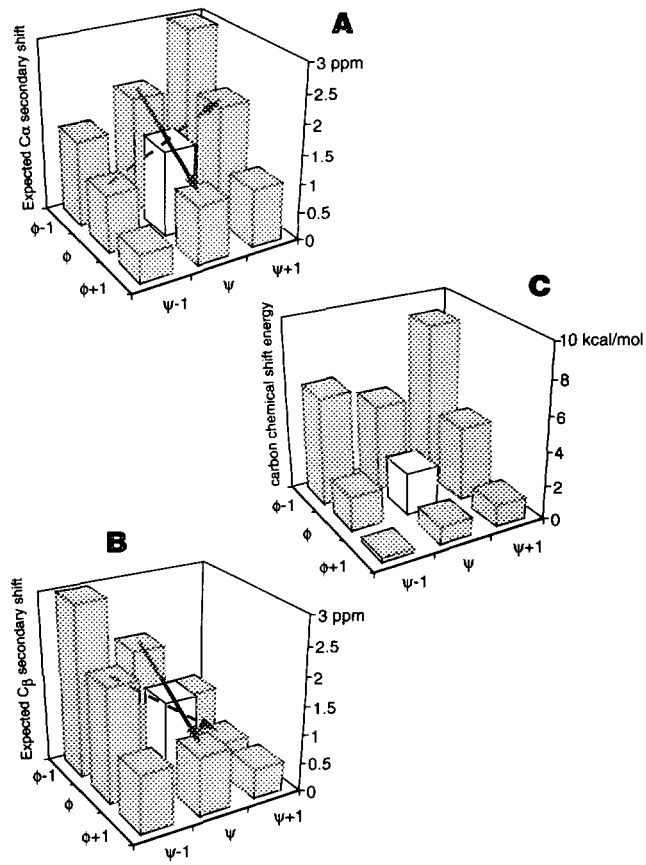

FIG. 1. Example of the calculation of the carbon chemical-shift energy and forces. (A) Sample expected C^{α} secondary chemical-shift data shown at the nine grid points centered about the point (ϕ, ψ), shown in white, at which the carbon chemical-shift energy is to be evaluated; the lines whose slopes approximate the partial derivatives of the C^{α} expectation value with respect to ϕ and ψ (see text) are shown by solid and dashed arrows, respectively. (B) Sample expected C^{β} secondary chemical-shift data at the same nine grid points; the lines whose slopes approximate the partial derivatives of the C^{β} expectation value with respect to ϕ and ψ (see text) are again shown by solid and dashed arrows, respectively. (C) Sample carbon chemical-shift energies at the same nine grid points, which have been calculated from the expected C^{α} and C^{β} chemical shifts, assuming that the observed C^{α} secondary shift = 0 ppm, the observed C^{β} secondary shift = 1 ppm, and k_{Cshift} = 1 kcal mol^{-1} ppm^{-2}.

derivatives of the square-well energy are still calculated using Eqs. [10] and [11], but with the terms corresponding to the carbon atom whose shift is within the specified errors set to zero. These square-well derivatives are valid at all points if $\text{error}^n > 0$, since the singularity at $|\Delta C^n| = 0$ is within the range where the derivatives are forced to be zero.

Since there is no explicit function fitted to the expectation values, the partial derivatives of $C^{\alpha}_{\text{expected}}$ and $C^{\beta}_{\text{expected}}$ with respect to ϕ and ψ are approximated by the local slopes of the expectation value grid about the grid point (ϕ, ψ) at which the energy is evaluated, as follows:

$$\delta C^{\alpha}_{\text{expected}}/\delta\phi(\phi,\psi) \approx [C^{\alpha}_{\text{expected}}(\phi+1,\psi) - C^{\alpha}_{\text{expected}}(\phi-1,\psi)]/2 \quad [12]$$

$$\delta C^{\beta}_{\text{expected}}/\delta\phi(\phi,\psi) \approx [C^{\beta}_{\text{expected}}(\phi+1,\psi) - C^{\beta}_{\text{expected}}(\phi-1,\psi)]/2 \quad [13]$$

$$\delta C^{\alpha}_{\text{expected}}/\delta\psi(\phi,\psi) \approx [C^{\alpha}_{\text{expected}}(\phi,\psi+1) - C^{\alpha}_{\text{expected}}(\phi,\psi-1)]/2 \quad [14]$$

$$\delta C^{\beta}_{\text{expected}}/\delta\psi(\phi,\psi) \approx [C^{\beta}_{\text{expected}}(\phi,\psi+1) - C^{\beta}_{\text{expected}}(\phi,\psi-1)]/2. \quad [15]$$

The implementation of this procedure for calculating the chemical-shift energy and partial derivatives to be evaluated at a point (ϕ, ψ), shown in white, is illustrated schematically in Fig. 1. Figure 1A shows the C^{α} secondary shift expectation

TABLE 1
Structural Statistics for the Original and C^{α}/C^{β} Chemical-Shift-Refined Structures of Reduced and Oxidized Human Thioredoxin (hTRX)[a]

	Reduced hTRX			Oxidized hTRX		
		Chemical-shift-refined			*Chemical-shift-refined*	
	Original	Harmonic potential	Square-well potential	Original	Harmonic potential	Square-well potential
rms deviations from carbon chemical shifts[b]						
δC^{α} (ppm)	1.23 ± 0.01	1.03 ± 0.03	1.12 ± 0.01	1.27 ± 0.02	1.05 ± 0.03	1.13 ± 0.02
δC^{β} (ppm)	1.13 ± 0.02	0.94 ± 0.02	1.01 ± 0.01	1.17 ± 0.02	0.94 ± 0.03	1.02 ± 0.01
rms deviations from experimental restraints[a]						
Interproton distances (Å)	0.008 ± 0	0.013 ± 0.001	0.013 ± 0.001	0.006 ± 0	0.010 ± 0.001	0.010 ± 0.001
Torsion angles (°)	0.160 ± 0.015	0.193 ± 0.038	0.198 ± 0.030	0.160 ± 0.024	0.219 ± 0.032	0.251 ± 0.042
$^3J_{\text{HN}\alpha}$ couplings (Hz)	0.33 ± 0.008	0.42 ± 0.04	0.41 ± 0.01	0.31 ± 0.009	0.43 ± 0.04	0.42 ± 0.01
E_{LJ} (kcal mol^{-1})[c]	−493 ± 7	−506 ± 9	−504 ± 8	−479 ± 7	−492 ± 7	−493 ± 8
rms deviations from idealized geometry						
Bonds (Å)	0.003 ± 0	0.004 ± 0	0.004 ± 0	0.003 ± 0	0.004 ± 0	0.004 ± 0
Angles (°)	0.480 ± 0.003	0.506 ± 0.008	0.514 ± 0.009	0.475 ± 0.005	0.508 ± 0.008	0.511 ± 0.008
Improper torsions (°)	0.227 ± 0.003	0.273 ± 0.012	0.289 ± 0.015	0.225 ± 0.004	0.285 ± 0.012	0.297 ± 0.014

[a] The original structures are from Qin *et al.* (*9*) and are based on a total of 2933 and 3018 experimental NMR restraints for the reduced and oxidized forms of human thioredoxin (hTRX), respectively. The breakdown of the experimental restraints is as follows: 2571 experimental distance restraints, 273 torsion angle restraints, and 89 $^3J_{\text{HN}\alpha}$ coupling constant restraints for reduced hTRX and 2649 experimental distance restraints, 278 torsion angle restraints, and 91 $^3J_{\text{HN}\alpha}$ coupling constant restraints for oxidized hTRX. All the structures were calculated using the simulated annealing protocol of Nilges *et al.* (*11*) with minor modifications using the program XPLOR (*7, 8*). The force constants employed for the chemical-shift term were 0.5 kcal mol^{-1} ppm^{-2} for the harmonic potential and 1.5 kcal mol^{-1} ppm^{-2} for the square-well potential. The force constants employed for the other terms are as follows: 50 kcal mol^{-1} Å^{-2}, 200 kcal mol^{-1} rad^{-2}, and 1 kcal mol^{-1} Hz^{-2} for the interproton distance (NOE), torsion angle, and coupling constant restraint terms, respectively; 4 kcal mol^{-1} Å^{-4} for the quartic van der Waals repulsion term with the hard sphere van der Waals radii set to 0.8 times their values in the CHARMM PARAM19/PARAM20 energy parameters (*12*); and 500 kcal mol^{-1} Å^{-2} for bonds and 500 kcal mol^{-1} rad^{-2} for angle (bond angles and improper torsions) terms. The potentials for the NOE and torsion angle restraints are quadratic square wells, while the potentials for covalent geometry and $^3J_{\text{HN}\alpha}$ coupling constants are harmonic. The improper torsion terms serve to maintain planarity and chirality.

[b] All C^{α} and C^{β} chemical shifts are included in the refinement with the exception of the shifts for the two cysteine residues (Cys32 and Cys35) and the single histidine (His44) and tryptophan (Trp31) residues. The Cys and His residues were not included as they were left out of the Spera and Bax (*1*) database. Trp31 was excluded as the large secondary shift of its C^{α} atom is apparently the result of other electronic effects. Specifically, the difference between observed and expected secondary shifts for Trp31 is 6.8–6.9 ppm, with an observed value of ~4 ppm and an expected value of 2.8 to 2.9 ppm. In contrast, the difference between the observed and the expected secondary shifts for the C^{β} of Trp31 is small (~0.48 ppm for reduced hTRX and 1.3 ppm for oxidized hTRX).

[c] E_{LJ} is the Lennard-Jones van der Waals energy calculated with the CHARMM empirical energy function (*12*). It is *not* included in the target function for simulated annealing.

grid (with arbitrary values) for the area around (ϕ, ψ). The solid arrow represents the approximate partial derivative of the expected C^α value with respect to ϕ [i.e., the slope of $C^\alpha_{\text{expected}}$ between the grid points ($\phi - 1$, ψ) and ($\phi + 1$, ψ)]. The dashed arrow represents the corresponding partial derivative of $C^\alpha_{\text{expected}}$ with respect to ψ [i.e., the slope of $C^\alpha_{\text{expected}}$ between the points (ϕ, $\psi - 1$) and (ϕ, $\psi + 1$)]. Figure 1B shows an expected C^β secondary shift grid, with the approximate partial derivatives of $C^\beta_{\text{expected}}$ with respect to ϕ and ψ again shown in solid or dashed arrows, respectively. Finally, Fig. 1C shows the value of the harmonic carbon chemical-shift energy calculated at each of the points which surround (ϕ, ψ), assuming for this example that k_{Cshift} = 1 kcal mol^{-1} ppm^{-2}, $C^\alpha_{\text{observed}}$ = 0 ppm, and $C^\beta_{\text{observed}}$ = 1 ppm.

In cases where there are no published expectation values of C^α and C^β secondary shifts for the grid point closest to the actual ϕ and ψ angles, no energy or forces are calculated. In addition, neither energy nor forces are calculated for cysteine and histidine residues, which Spera and Bax (*1*) deleted from their starting database.

To assess the impact of direct C^α and C^β chemical-shift refinement, we used the procedure outlined above to further refine the structures of reduced and oxidized human thioredoxin, recently published by Qin *et al.* (*9*). The original ensemble of structures (comprising 40 simulated annealing structures for both the reduced and the oxidized forms) were based on an average of about 29 experimental NMR restraints per residue and are among the most precise and accurate protein structures determined by NMR (*10*). The new ensemble of structures, incorporating carbon chemical shifts directly into the refinement, were calculated using the simulated annealing protocol of Nilges *et al.* (*11*) with only minor modifications. The results of direct chemical-shift refinement are summarized in Tables 1 and 2, which present the structural statistics and atomic rms differences, respectively. The agreement with the observed C^α and C^β chemical shifts for the original set of structures is 1.2–1.3 ppm and 1.1–1.2 ppm, respectively (Table 1). This is comparable to the agreement between the observed $\delta(\phi, \psi)$ values and the expected $\Delta(\phi, \psi)$ surface obtained for four highly refined protein crystal structures, where the rms deviation was 1.10 ppm for C^α and 1.14 ppm for C^β (*1*). One can therefore conclude that the quality of the original NMR structures is similar to that of the X-ray structures employed in the database. When the original structures are subjected to chemical-shift refinement, the agreement with the observed C^α and C^β secondary shifts is improved by approximately 16–20% with the harmonic chemical-shift potential and by about 9–13% with the square-well potential (Table 1). Although this is accompanied by a slight decrease in the agreement between the observed and the calculated values of the other experimental NMR restraints (i.e., approximate interproton distances, torsion angles, and $^3J_{\text{HN}\alpha}$ coupling constants), this cannot be regarded as significant as the differences remain well within experimental error (Table 1). In addition, the quality of the nonbonded contacts (assessed independently by calculating the Lennard–Jones van der Waals energy) and the deviations from idealized covalent geometry remain essentially unaffected (Table 1). Similarly, the precision of the structures is also not affected in any significant way, and the atomic rms shifts accompanying chemical-shift refinement are sufficiently small that the new and old ensembles of structures overlap (that is, the difference between the mean coordinates of the original and chemical-shift-refined ensembles is smaller than the average rms difference between the individual structures and the mean coordinates for each ensemble) (see Table 2).

TABLE 2
Atomic rms Differences[a]

	Atomic rms difference (Å)					
	Reduced hTRX			Oxidized hTRX		
	Backbone atoms	All atoms	All ordered atoms[b]	Backbone atoms	All atoms	All ordered atoms[b]
$\langle SA_{ori} \rangle$ vs $\overline{SA}_{ori}$	0.19 ± 0.02	0.60 ± 0.03	0.30 ± 0.02	0.18 ± 0.02	0.58 ± 0.03	0.31 ± 0.03
$\langle SA_{\delta har} \rangle$ vs $\overline{SA}_{\delta har}$	0.23 ± 0.03	0.63 ± 0.04	0.35 ± 0.03	0.23 ± 0.03	0.60 ± 0.04	0.35 ± 0.03
$\langle SA_{\delta squ} \rangle$ vs $\overline{SA}_{\delta squ}$	0.23 ± 0.03	0.63 ± 0.04	0.36 ± 0.03	0.24 ± 0.02	0.60 ± 0.03	0.36 ± 0.03
$\overline{SA}_{\delta har}$ vs $\overline{SA}_{ori}$	0.19	0.27	0.22	0.21	0.28	0.23
$\overline{SA}_{\delta squ}$ vs $\overline{SA}_{ori}$	0.20	0.26	0.23	0.21	0.27	0.23

[a] The notation of the hTRX structures is as follows: $\langle SA_{ori} \rangle$, $\langle SA_{\delta har} \rangle$, and $\langle SA_{\delta squ} \rangle$ are the ensemble of original, chemical-shift-refined with harmonic potential, and chemical-shift-refined with square-well potential structures, respectively. There are 40 individual structures in each ensemble. $\overline{SA}_{ori}$, $\overline{SA}_{\delta har}$, and $\overline{SA}_{\delta squ}$ are the mean coordinates obtained by averaging the coordinates of the individual structures in the $\langle SA_{ori} \rangle$, $\langle SA_{\delta har} \rangle$, and $\langle SA_{\delta squ} \rangle$ ensembles, respectively.

[b] The list of ordered atoms is given in the paper by Qin *et al.* (*9*) describing the original structures.

The small atomic rms shifts obtained upon chemical-shift refinement for the two examples presented above are easily explained. The restraints used to calculate the original ensemble of structures included $^3J_{HN\alpha}$ coupling constants for 86–88% of the residues (*9*). As a result, the ϕ backbone torsion angles for these residues are defined to high accuracy. As the ψ backbone torsion angles are highly correlated to ϕ, it is not surprising to find good agreement with the observed secondary shifts in the original ensemble of structures. The additional improvement upon chemical-shift refinement is therefore mainly due to residues for which no $^3J_{HN\alpha}$ coupling constants were available.

In conclusion, the incorporation of $^{13}C^{\alpha}$ and $^{13}C^{\beta}$ secondary chemical shifts directly into the refinement procedure offers a useful additional set of restraints in protein structure determination by NMR. Although the information is to some extent redundant with that offered by $^3J_{HN\alpha}$ coupling constants, the two experimental measures are complementary. Thus, the values of the $^3J_{HN\alpha}$ coupling constants depend only on ϕ, whereas the $^{13}C^{\alpha}$ and $^{13}C^{\beta}$ chemical shifts are dependent on both ϕ and ψ. Moreover, $^3J_{HN\alpha}$ coupling constants may not be measurable for all residues, due to small values of the couplings, to line broadening, or to chemical-shift overlap of the backbone nitrogen atoms. In contrast, $^{13}C^{\alpha}$ and $^{13}C^{\beta}$ shifts are readily obtained for almost all residues. Thus, for both the reduced and the oxidized forms of thioredoxin, for example, $^3J_{HN\alpha}$ coupling constants could not be obtained for residues within the active site owing to line broadening of the NH resonances; the incorporation of the carbon chemical-shift restraints resulted in a backbone atomic rms shift for residues 30–37, which form the active site together with one residue on either side of it, of 0.25 Å for the reduced form and 0.06 Å for the oxidized form. Finally, the computational cost of incorporating $^{13}C^{\alpha}$ and $^{13}C^{\beta}$ chemical-shift restraints is negligible (less than a 1% increase in the CPU time required for simulated annealing refinement).

ACKNOWLEDGMENTS

This work was supported by the AIDS Targeted Anti-Viral Program of the Office of the Director of the National Institutes of Health (to G.M.C. and A.M.G.). We thank Ad Bax for numerous discussions and for providing the $C^{\alpha,\beta}_{expected}$ C (ϕ, ψ) surfaces and the corresponding error surfaces.

REFERENCES

1. S. Spera and A. Bax, *J. Am. Chem. Soc.* **113,** 5491 (1991).
2. D. S. Wishart, F. M. Richards, and B. D. Sykes, *J. Mol. Biol.* **222,** 311 (1991).
3. D. S. Wishart and B. D. Sykes, *J. Biomol. NMR* **4,** 171 (1994).
4. A. C. de Dios, J. G. Pearson, and E. Oldfield, *Science* **260,** 1491 (1993).
5. A. C. de Dios, J. G. Pearson, and E. Oldfield, *J. Am. Chem. Soc.* **115,** 9768 (1993).
6. D. S. Garrett, J. Kuszweski, T. J. Hancock, P. J. Lodi, G. W. Vuister, A. M. Gronenborn, and G. M. Clore, *J. Magn. Reson. B* **104,** 99 (1994).
7. A. T. Brünger, G. M. Clore, A. M. Gronenborn, and M. Karplus, *Proc. Natl. Acad. Sci. USA* **83,** 3801 (1986).
8. A. T. Brünger, "X-PLOR Version 3.0 Manual," Yale University, New Haven, Connecticut, 1992.
9. J. Qin, G. M. Clore, and A. M. Gronenborn, *Structure* **2,** 503 (1994).
10. G. M. Clore and A. M. Gronenborn, *Protein Sci.* **3,** 372 (1994).
11. M. Nilges, G. M. Clore, and A. M. Gronenborn, *FEBS Lett.* **229,** 317 (1988).
12. B. R. Brooks, R. E. Bruccoleri, B. D. Olafson, D. J. States, S. Swaminathan, and M. Karplus, *J. Comput. Chem.* **4,** 187 (1983).